

Understanding Cross-Task Generalization in Handwriting-Based Alzheimer’s Screening via Vision-Language Adaptation

Changqing Gong, Huafeng Qin and Mounîm A. El-Yacoubi

Abstract—Alzheimer’s disease (AD) is a prevalent neurodegenerative disorder for which early detection is critical. Handwriting—often disrupted in prodromal AD—provides a non-invasive and cost-effective window into subtle motor and cognitive decline. Existing handwriting-based AD studies, mostly relying on online trajectories and hand-crafted features, have not systematically examined how task type influences diagnostic performance and cross-task generalization. Meanwhile, large-scale vision-language models (VLMs) have demonstrated remarkable zero/few-shot anomaly detection in natural images and strong adaptability across medical modalities such as chest X-ray and brain MRI. However, handwriting-based disease detection remains largely unexplored within this paradigm. To close this gap, we introduce a lightweight **Cross-Layer Fusion Adapter** (CLFA) framework that repurposes CLIP for handwriting-based AD screening. CLFA implants multi-level fusion adapters within the visual encoder to progressively align representations toward handwriting-specific medical cues, enabling prompt-free and efficient zero-shot inference. Using this framework, we systematically investigate cross-task generalization—training on a specific handwriting task and evaluating on unseen ones—to reveal which task types and writing patterns most effectively discriminate AD. Extensive analyses further highlight characteristic stroke patterns and task-level factors that contribute to early AD identification, offering both diagnostic insights and a benchmark for handwriting-based cognitive assessment.

Index Terms—Alzheimer’s disease, Computer-aided diagnosis, Handwriting Analysis, Deep Learning, CLIP.

I. INTRODUCTION

Alzheimer’s disease (AD), the most common cause of dementia, is a progressive neurodegenerative disorder characterized by gradual nerve cell degeneration and cognitive decline in memory, reasoning, and daily functioning [1, 2, 3, 4, 5]. Similar conditions, including Lewy body disease, frontotemporal degeneration, Parkinson’s disease, and stroke, also impair cognitive function, with incidence increasing with age [6, 7, 8, 9, 10]. Although incurable, early detection and timely intervention can slow progression [11]. However, costly and/or invasive biomarkers (e.g., A-PET, cerebrospinal fluid

Changqing Gong and Mounîm A. El-Yacoubi are with Telecom SudParis, Institut Polytechnique de Paris, 91120 Palaiseau, France (e-mail: changqing.gong@telecom-sudparis.eu; mounim.el_yacoubi@telecom-sudparis.eu).

Huafeng Qin is with the School of Computer Science and Information Engineering, Chongqing Technology and Business University, Chongqing 400067, China (e-mail: qinhuafengfeng@163.com).

Manuscript received xx; revised xx; accepted xx. This work was supported in part by xxx, and in part by xxx. We also would like to thank Telecom SudParis and Institut Polytechnique de Paris for their partial support (Corresponding author: Mounîm A. El-Yacoubi.)

testing) [12] and subjective neuropsychological tests (e.g., MMSE, MoCA) [13] hinder large-scale early screening.

To expand accessible biomarkers, researchers have explored signals sensitive to cognitive decline, including eye movement [14], speech [15], galvanic skin response [16], Gait disturbances and frailty [17, 18, 19, 20]. Handwriting—which jointly engages cognitive planning and fine motor control—offers a non-invasive, low-cost window into disease-related changes [21, 22, 23]. With graphic tablets, online handwriting tasks can be administered easily while capturing kinematic and dynamic data for automated analysis [24]. Recent studies report that handwriting is often impaired in prodromal AD [1, 25, 26, 27, 21], and machine learning (ML) can reduce clinical assessment time in motor-function evaluation [28].

Most handwriting-based AD studies—predominantly using online handwriting—rely on hand-crafted features with shallow classifiers [1, 29, 30, 31]. Although recent deep learning (DL) approaches often outperform hand-engineered pipelines across vision tasks and have been explored for handwriting-based AD detection using either 1D-CNNs on temporal signals or 2D-CNNs on rendered images [32, 33, 34], as well as a hybrid Transformer that integrates 2D handwriting images with 1D signal features for early AD detection [35].

Despite promising results, few works have systematically examined how handwriting task affects both in-domain performance and cross-task generalization. Recently, large-scale pre-trained visual-language models (VLM) have witnessed substantial advancements, applied to many different scenarios [36, 37, 38]. VLM has delivered impressive zero/few-shot anomaly detection in natural images [39, 40, 41, 42], and strong performance across several medical imaging modalities [43] (e.g., chest X-ray, brain MRI, histopathology, retinal OCT). However, to our knowledge, handwriting-based disease detection remains largely unexplored within the VLM paradigm. In particular, the zero-shot setting—training on a limited subset of handwriting tasks or exemplars and evaluating on previously unseen tasks or cohorts—has received little attention in handwriting-based AD screening, leaving open questions about task-transferability and out-of-distribution robustness. Task transferability and out-of-distribution robustness of handwriting tasks have not been systematically studied, the potential of VLM in this field has not yet been explored.

To close this gap, we introduce **Cross-Layer Fusion Adapters** (CLFA), a lightweight multi-level adapter framework that repurposes CLIP for handwriting-based AD detection. At several depths of the ViT image encoder, we implant

residual fusion adapters that (i) project tokens into a compact bottleneck, (ii) apply a depthwise 1D convolution along the token sequence to capture local patch context, and (iii) fuse the current-layer descriptor with the already-fused descriptor propagated from the preceding adapter. The fused descriptor is then mapped back to the backbone width and injected as a small residual update, progressively retargeting the visual features from natural-image semantics to handwriting-specific medical cues while keeping the CLIP backbone largely intact. The fused mid-level descriptors at each tapped layer are treated as patch-level “detection tokens” and compared to normal/abnormal CLIP text prototypes, with multi-level aggregation yielding image-level anomaly scores for zero-shot screening.

- **Cross-Layer Fusion Adapters.** We present the first CLIP-based lightweight adapter framework for zero-shot handwriting-based Alzheimer’s disease (AD) detection. The proposed design employs a multi-level in-network fusion strategy, where each adapter merges current-layer tokens with the previously fused descriptor and injects a small residual update, progressively aligning representations with handwriting-specific cues.
- **Tokenwise depthwise 1D adaptation.** Each lightweight adapter adopts a pointwise–depthwise–pointwise structure. The depthwise 1D convolution efficiently captures local token context and stroke dependencies with minimal parameters and computation. Adapter outputs are injected with a small residual coefficient, preserving the pretrained model’s representational capacity while gently steering features toward handwriting-related evidence.
- **Comprehensive zero-shot evaluation and generalization.** On the DARWIN benchmark, we conduct systematic zero-shot detection across diverse task-combination protocols, establishing a strong reference for handwriting-based AD screening. Cross-dataset and unseen-task experiments further demonstrate robustness beyond the training distribution.

Next, Section 2 reviews the state of the art. Section 3 outlines the DARWIN dataset tasks and data preprocessing. Section 4 details our proposed model and loss functions. Section 5 presents our experiments, comparing results with state-of-the-art models and analyzing the findings.

II. RELATED WORK

Deterioration in writing ability is a recognized indicator of AD [25], and kinematic handwriting analyses have revealed pathological patterns during the writing process [1]. Handwriting-based AD detection spans traditional machine learning (ML) and deep learning (DL). Classical ML approaches extract temporal, kinematic, and spatial descriptors (e.g., speed, pressure, curvature) and train shallow classifiers such as logistic regression, SVMs, decision trees, or random forests [30, 31, 44, 45]. These methods, while interpretable, often depend on extensive feature engineering and dataset-specific tuning.

DL has accelerated handwriting-based screening for neurodegenerative disorders, notably Parkinson’s Disease (PD)

and, to a lesser extent, AD. Several studies transform 1D pen signals into 2D representations and apply CNN-based models [46, 47, 48]. For AD, [45] introduced the DARWIN dataset; subsequent works combine handcrafted or CNN-derived image features with ML heads [49, 50, 34], and explore 1D-CNNs with data augmentation for early-stage detection [32]. In addition, 2D handwriting images were integrated with 1D feature signals [35], enhancing the ability to capture the multimodal characteristics of handwriting.

To the best of our knowledge, no research has explored the abnormal detection of AD based on handwriting. In contrast, the industrial anomaly detection community has progressed rapidly: recent works such as WinCLIP[51] leverage foundation models for zero-/few-shot inspection by harnessing language guidance, [52] proposed a multimodal anomaly detection method using cross-modal mappings between frozen 2D and 3D features, detecting anomalies via discrepancies at inference. [53] addressed open-set supervised anomaly detection (OSAD) by learning heterogeneous anomaly distributions from limited anomalies to handle unseen cases. [39] introduced InCTRL, a generalist anomaly detection approach that applies contextual residual learning and few-shot exemplars for cross-domain anomaly detection..

Translating these ideas to medical anomaly detection is substantially more challenging due to larger domain gaps across modalities and cohorts. Current medical AD approaches typically cast detection as one-class classification, training only on normal images [54, 55, 56, 57, 58]. Leveraging pre-trained CLIP models for language-guided detection and segmentation has emerged as an effective strategy. [59, 60] achieved promising results in this direction. [43] further extended the application of VLM, originally trained on natural images, by introducing a distinctive framework for multi-level visual feature adaptation and comparison.

Notably, the zero-shot regime—training on limited handwriting tasks or exemplars and evaluating on previously unseen tasks or cohorts—has received little attention. To address this gap, we repurpose a pre-trained vision–language model to build a novel handwriting AD anomaly detector and systematically evaluate cross-task generalization, enabling an analysis of which handwriting factors most strongly relate to AD-linked anomalies. These gaps motivate our study: repurposing a vision–language pretrained (VLP) model for handwriting-based AD, with a deployment-friendly, zero-text testing paradigm and strong cross-task generalization.

III. MATERIAL AND METHOD

In this section, we introduce the dataset, describe our preprocessing of raw signal data, the extraction of 1D signal features and the reconstruction of handwriting images.

A. Dataset

We used the DARWIN-RAW dataset [45], a gold-standard resource for AD diagnosis, with data from 174 participants (89 AD patients and 85 healthy controls). This dataset includes 25 handwriting tasks designed for early AD detection [24], categorized into three types: memory and dictation (M), Copy

(C), and Graphic (G). The raw handwriting data (x_i, y_i, p_i) were preprocessed to generate 2D images. This process was motivated by the effectiveness of kinematic features in detecting early AD.

B. Generation of 2D Images from Online Handwriting

Our preprocessing and 1D feature extraction steps largely follow the protocol in [35], including handling of missing values, interpolation, outlier removal, and the derivation of kinematic descriptors such as velocity, acceleration, jerk, curvature, and pressure. For details, we refer the reader to [35].

Building on these signals, we render 2D trajectory images by segmenting each task into *paper* (pen-contact), *air* (in-air), and *all* (full trajectory) streams. Trajectories are min–max normalized to a fixed canvas and rasterized with distance-adaptive interpolation. The RGB channels encode distinct handwriting dynamics: curvature (R), velocity (G), and jerk (B). Stroke thickness is modulated by pen pressure, while dominant frequency—estimated from the velocity spectrum—acts as a global intensity boost to emphasize tremor-related micro-oscillations. In this paper, we use only the handwriting on the paper as our research subject. Examples of generated images are shown in Figure 1.

C. Language Feature Formatting

Motivated by prior work on prompt ensembling [43, 51], we construct normal/abnormal text prototypes with a two-tier scheme to reduce prompt sensitivity.

Inspired by prior work on prompt ensembles, we construct normal/abnormal text prototypes using a two-layer scheme to reduce prompt sensitivity. As shown in Table I, we provide concise descriptions for 25 handwriting tasks by simplifying the task definitions in [45]. To obtain natural-language descriptions and task abbreviations, we further condense the wording; as summarized in Table II, we employ a compact library of handwriting-quality descriptors for the two states (normal, abnormal), rather than a single generic sentence.

Each pattern contains a slot that is instantiated with the task-specific noun phrase from Table III, yielding phrases such as “clear signature.” At the template layer, we adopt a set of hand-crafted templates [43] and compute the mean of their embeddings. Finally, for task t , the normal/abnormal prototypes are collected as

$$\mathbf{E}_t = [\mathbf{e}_t^{\text{nor}}, \mathbf{e}_t^{\text{abn}}] \in \mathbb{R}^{T \times 2}. \quad (1)$$

IV. PROPOSED WORK

Handwriting-based AD screening requires models that can generalize across heterogeneous writing tasks while remaining lightweight and prompt-free at inference. To this end, we repurpose CLIP through a Cross-Layer Fusion Adapter (CLFA) framework that progressively adapts the pretrained vision backbone to handwriting-specific medical cues. CLFA implants multi-level adapters within the visual encoder. Each adapter performs tokenwise depthwise convolution and cross-layer fusion, yielding locally contextualized and hierarchically aligned representations suitable for zero-shot AD detection.

TABLE I
TEXT PROMPT TASK NAMES

ID	Task name	ID	Task name
1	signature	2	horizontal line drawing
3	vertical line drawing	4	large circle drawing
5	small circle drawing	6	copied letter ‘L’ ‘M’ ‘P’
7	copied letters	8	cursive letter writing
9	cursive bigram writing	10	copied word ‘foglio’
11	copied word ‘foglio’ on line	12	copied word ‘mamma’
13	copied word ‘mamma’ on line	14	written memory words
15	reversed word ‘bottiglia’	16	reversed word ‘casa’
17	copied multi-word phrases	18	written object name
19	postal form copy	20	dictated sentence writing
21	complex shape drawing	22	copied phone number
23	dictated phone number writing	24	hand-drawn clock
25	paragraph transcription		

TABLE II
STATE-LEVEL PROMPTS FOR NORMAL AND ABNORMAL HANDWRITING QUALITY.

Normal	Abnormal
[o]	distorted [o]
clear [o]	unclear [o]
well-written [o]	trembled [o]
legible [o]	impaired [o]
neatly drawn [o]	[o] with shaky lines
[o] with normal	[o] with abnormal
healthy [o]	poorly written [o]

A. Problem Setup and Notation

We aim to repurpose a vision–language model trained on natural images, denoted M_{nat} (e.g., CLIP), for image-level anomaly detection in handwriting, yielding an adapted model M_{ad} . Adaptation uses a handwriting training set $\mathcal{D}_{\text{train}}$ drawn from multiple writing tasks, while evaluation targets unseen tasks under a zero-shot protocol.

Let $\mathcal{D}_{\text{train}} = \{(x_i, c_i, t_i)\}_{i=1}^K$, where $x_i \in \mathbb{R}^{h \times w \times 3}$ is a handwriting image, $c_i \in \{0, 1\}$ is the image-level anomaly label (0 normal, 1 abnormal), and $t_i \in \mathcal{T}_{\text{train}}$ is the task identity. The test set $\mathcal{D}_{\text{test}}$ is built from tasks $\mathcal{T}_{\text{test}}$ that are disjoint from training tasks, i.e., $\mathcal{T}_{\text{train}} \cap \mathcal{T}_{\text{test}} = \emptyset$.

For an input x , the visual backbone in M_{ad} produces token sequences at selected layers $\ell \in \mathcal{L}$: $\mathbf{X}^{(\ell)} \in \mathbb{R}^{N \times C}$ ($N = \text{CLS} + S$ patches). At each selected layer, our dual-head adapter outputs (i) a text-aligned patch descriptor and (ii) a residual update that is injected back into the backbone.

For each training task $t \in \mathcal{T}_{\text{train}}$, we precompute CLIP text prototypes $\mathbf{E}_t = [\mathbf{e}_t^{\text{nor}}, \mathbf{e}_t^{\text{abn}}] \in \mathbb{R}^{T \times 2}$ via prompt ensembles. In training, the cross-layer fusion adapters leverage text-prompt prototypes for patch-level alignment and detection guidance. The pretrained visual backbone is kept fixed, and only the lightweight adapters are optimized to adapt CLIP to handwriting data.

Given a test image x_{test} from an unseen task $t_{\text{test}} \in \mathcal{T}_{\text{test}}$, the model outputs an image-level anomaly score $s(x_{\text{test}}) \in [0, 1]$. Performance is reported under zero-shot transfer from $\mathcal{T}_{\text{train}}$ to $\mathcal{T}_{\text{test}}$, assessing robustness to previously unseen handwriting tasks and distributions.

B. Cross-Layer Fusion Adapters

In handwriting-based anomaly detection, local stroke continuity and subtle spatial variations are more critical than

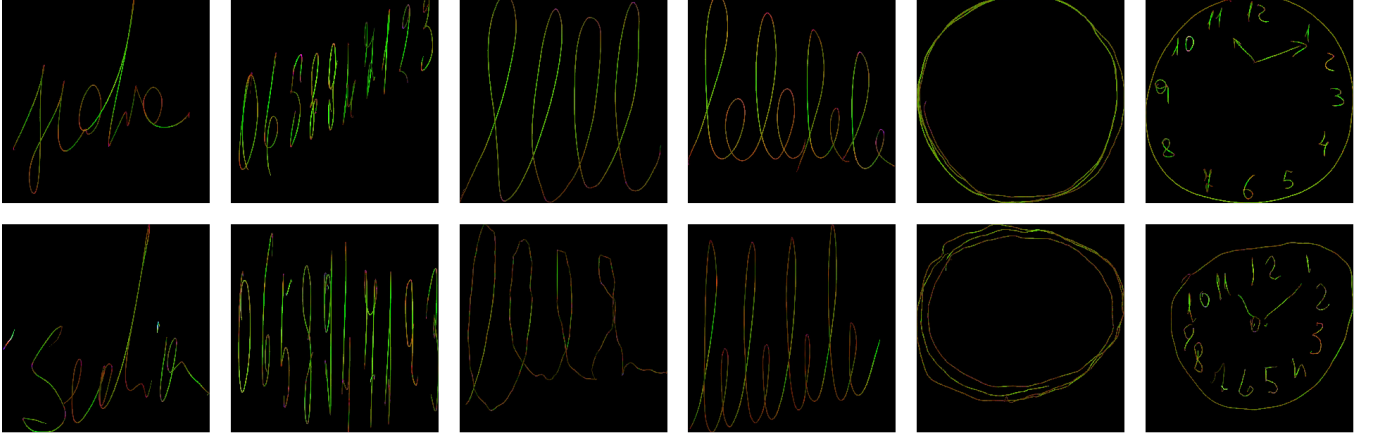


Fig. 1. Example trajectory images generated from online handwriting. Top row: healthy controls; bottom row: AD patients. We show representative samples from the three major task categories: memory/dictation (M: Task 14, Task 22), copying (C: Task 8, Task 9), and graphic drawing (G: Task 4, Task 24). While some handwriting impairments in AD subjects are relatively easy to diagnose (e.g., distorted or trembled strokes), others remain subtle and difficult to distinguish from healthy controls, reflecting the variability of early-stage AD detection.

TABLE III
TEMPLATE-LEVEL PROMPTS FOR TEXT FEATURE ENSEMBLING.

Templates (examples)
a bad photo of a/the [c].
a good photo of a/the [c].
a black and white photo of a/the [c].
a low resolution photo of a/the [c].
a photo of one [c].
a dark photo of a/the [c].
a cropped photo of a/the [c].
a photo of a large [c].
a photo of a cool [c].
a bright photo of a/the [c].
a photo of the small [c].
a close-up photo of the [c].
a blurry photo of a/the [c].
a jpeg corrupted photo of a/the [c].
a photo of a/the [c].
there is a/the [c] in the scene.
this is a/the/one [c] in the scene.

high-level semantics. To this end, we use a cross-layer fusion mechanism that directly propagates mid-level cues across transformer blocks. Each adapter learns to refine its own token representation by integrating the fused descriptor from the previous layer, while a depthwise 1D convolution captures fine-grained contextual dependencies along the token sequence. This design yields efficient, interpretable, and self-contained adaptation.

Given an input image $x \in \mathbb{R}^{h \times w \times 3}$, the CLIP visual encoder produces token features at selected layers $\ell \in \mathcal{L}$: $\mathbf{X}^{(\ell)} \in \mathbb{R}^{N \times C}$, where N denotes the number of tokens (cls + $h \times w$ patches). At each selected layer, we implant a lightweight *Fusion Adapter* that generates (i) a compact patch descriptor and (ii) a residual update softly injected back into the visual stream, as illustrated in Figure 2.

a) *Adapter structure*: For layer ℓ , the adapter first projects token features into a bottleneck space ($T=768$), as shown in Eq.(2):

$$\mathbf{H}^{(\ell)} = \mathbf{X}^{(\ell)} \mathbf{W}_1, \quad (2)$$

where $\mathbf{W}_1 \in \mathbb{R}^{C \times T}$ and $\mathbf{H}^{(\ell)} \in \mathbb{R}^{N \times T}$. The projected tokens are then processed by a depthwise 1D convolution along the token sequence, which captures local contextual dependencies among nearby patches, as shown in Eq.(3):

$$\mathbf{M}'^{(\ell)} = \phi(\mathbf{H}^{(\ell)} + \text{DWConv1D}(\mathbf{H}^{(\ell)})), \quad (3)$$

where $\phi(\cdot)$ denotes the activation function (LeakyReLU).

b) *Cross-layer fusion*: As shown in Figure 3. To propagate fused information upward, each adapter (except the first) receives the fused descriptor $\mathbf{Z}^{(\ell-1)}$ from the previous adapter . The fusion process is defined as Eq.(4)

$$\mathbf{M}^{(\ell)} = \mathbf{M}'^{(\ell)} + \mathbf{Z}^{(\ell-1)} \mathbf{W}_z, \quad (4)$$

where $\mathbf{W}_z \in \mathbb{R}^{T \times T}$ is a learnable transformation applied to the preceding fused descriptor. Meanwhile, the fused output $\mathbf{M}^{(\ell)}$ is propagated upward as $\mathbf{Z}^{(\ell)}$ to serve as the input fusion term for the next adapter layer.

c) *Residual retargeting*: The fused descriptor is first mapped back to the original channel dimension through a lightweight projection, as shown in Eq.(5):

$$\mathbf{Y}^{(\ell)} = \phi(\mathbf{M}^{(\ell)} \mathbf{W}_2), \quad (5)$$

where $\mathbf{W}_2 \in \mathbb{R}^{T \times C}$ and $\phi(\cdot)$ denotes the activation function. The resulting output is then softly blended into the visual stream with a small residual coefficient:

$$\mathbf{X}_{\text{out}}^{(\ell)} = (1 - \alpha) \mathbf{X}^{(\ell)} + \alpha \mathbf{Y}^{(\ell)}, \quad (6)$$

where $\alpha=0.1$ in practice. As shown in Eq. (6), this residual injection gently steers the pretrained CLIP backbone toward handwriting-specific evidence without disrupting global semantics.

d) *Prototype matching and aggregation*: At each adapter depth, the fused descriptors are ℓ_2 -normalized and compared with the normal/abnormal CLIP text prototypes $\mathbf{E}_t \in \mathbb{R}^{T \times 2}$, as shown in Eq. (7) :

$$\mathbf{A}^{(\ell)} = \text{softmax}(\text{norm}(\mathbf{M}^{(\ell)})) \mathbf{E}_t \in \mathbb{R}^{N \times 2}. \quad (7)$$

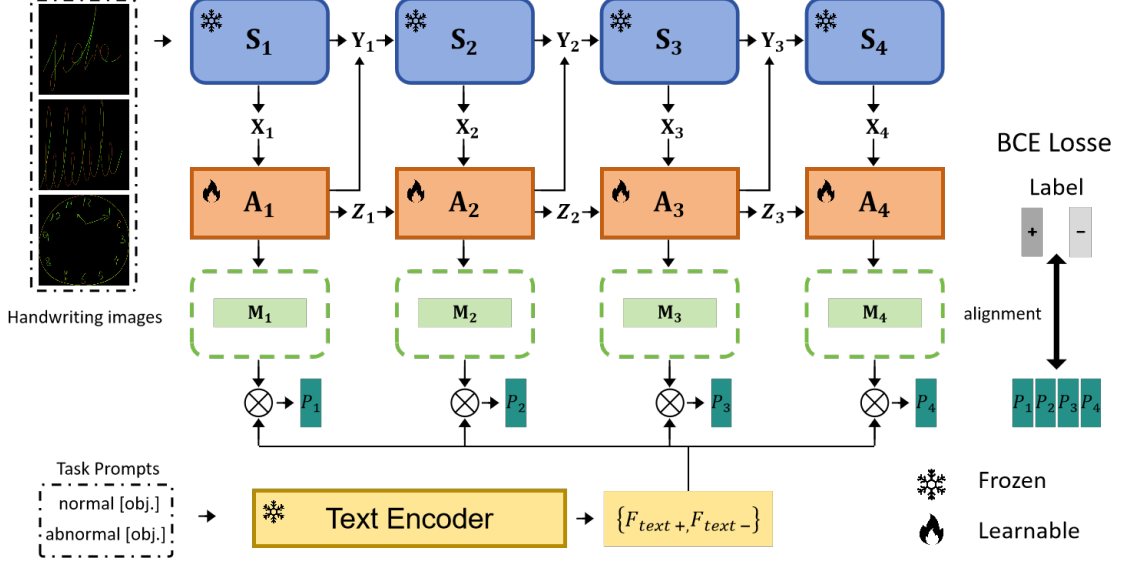


Fig. 2. Overview of the Cross-Layer Fusion Adapter (CLFA). Each selected ViT block hosts a lightweight adapter with depthwise 1D convolution and cross-layer fusion. Fused mid-level descriptors are compared to normal/abnormal CLIP text prototypes for zero-shot detection.

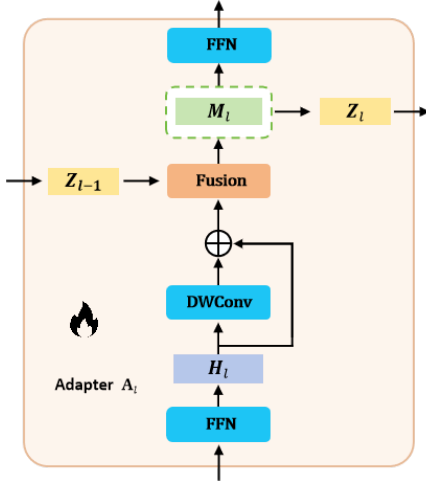


Fig. 3. Cross-layer fusion Adapter.

The abnormality probability for layer ℓ is obtained by pooling the abnormal channel, as shown in Eq. (8):

$$p^{(\ell)} = \text{Pool}(\mathbf{A}^{(\ell)}[:, 1]), \quad (8)$$

e) *Detection objective.*: The detection loss averages binary cross-entropy (BCE) over all selected layers, as shown in Eq. (9):

$$\mathcal{L}_{\text{det}} = \frac{1}{|\mathcal{L}|} \sum_{\ell \in \mathcal{L}} \text{BCE}(p^{(\ell)}, y), \quad (9)$$

where $y \in \{0, 1\}$ is the ground-truth label (normal vs. abnormal).

V. EXPERIMENTAL RESULTS AND DISCUSSION

In this section, we analyze the cross-task generalization behavior of handwriting-based Alzheimer's screening using our CLFA framework. Rather than focusing solely on absolute

detection performance, we aim to understand how handwriting task types influence zero-shot generalization and which task patterns best reveal Alzheimer-related impairments.

A. Experimental Setup

To assess our approach, we conducted extensive experiments on the DARWIN-RAW publicly available gold-standard dataset, collected using Wacom's Bamboo tablet from 174 participants. The x-y coordinate sequences of pen-tip movements were recorded at a frequency of 200 Hz. The dataset consists of x-y coordinates (174 subjects \times 25 tasks \times 1 x-y coordinate sequence, with some missing data). The x-y coordinates were then processed following the procedures described in Chapter 3. We utilize the CLIP with ViT-L/14 architecture, with input images at a resolution of 240. The model comprises a total of 24 layers, which are divided into 4 stages, each encompassing 6 layers. During training, we set the learning rate to 0.0001 and the batch size to 1. We use the Adam optimizer at a constant learning rate of 1e-3 and a batch size of 1. All experiments were conducted using the PyTorch framework on a computer equipped with NVIDIA™GPUs. For fairness, we set the image resolution to 240 \times 240 for all models. We regard state-of-the-art approaches MVFA [43] under same training configurations as competitive baselines. Beyond model training and evaluation, we emphasize task-wise cross-generalization, where a model trained on one handwriting task is tested on all others to quantify inter-task transferability.

B. Evaluation Metrics

The area under the receiver operating characteristic curve (AUC) was employed to quantify model performance. This metric is widely recognized as a standard criterion for anomaly detection. In the context of handwriting-based Alzheimer's disease detection, the dataset does not provide pixel-level abnormality masks. Therefore, we exclusively focus on image-level AUC as the evaluation measure.

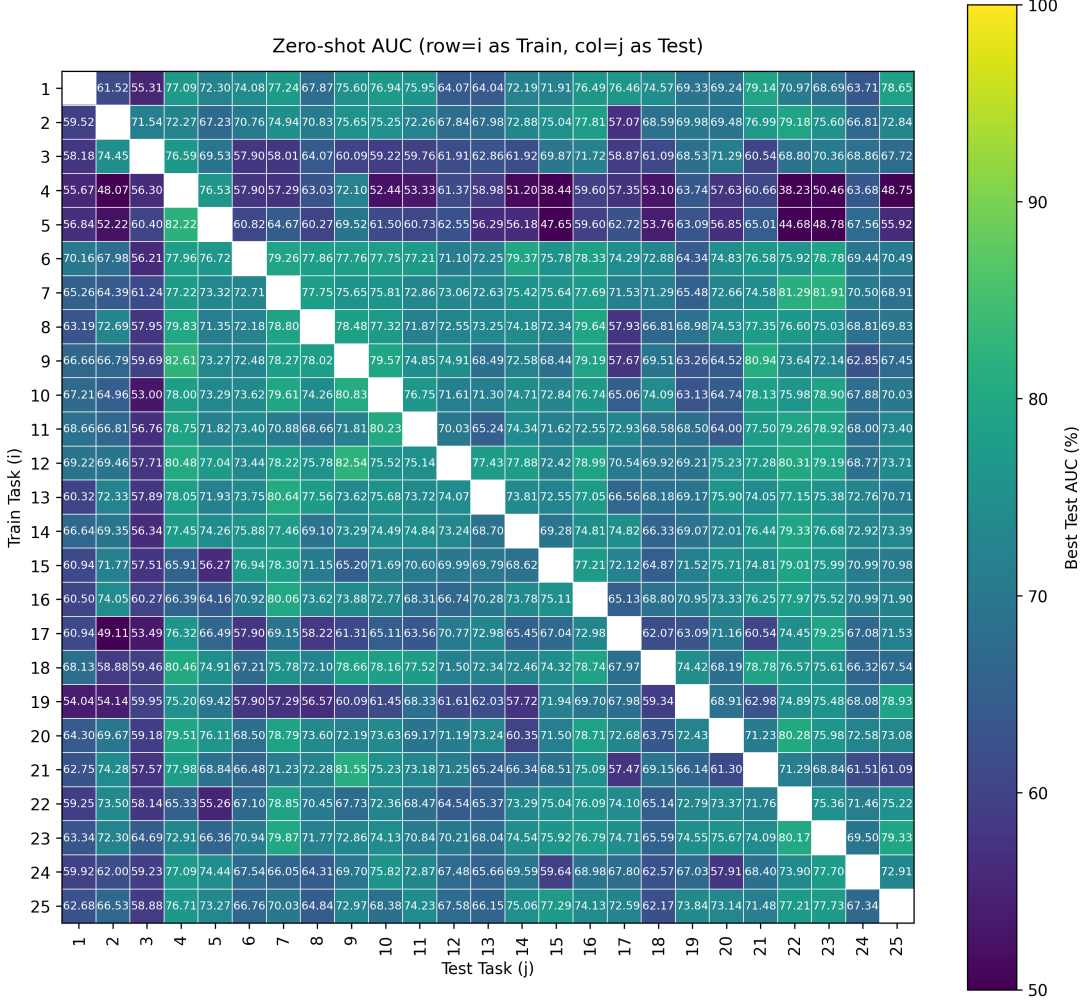


Fig. 4. Cross-task AUC matrix for zero-shot AD detection using CLFA. Rows denote training tasks; columns denote testing tasks. Higher off-diagonal values indicate stronger cross-task generalization.

C. Adapter Architecture Configuration

The main architectural configurations of our Cross-Layer Fusion Adapter (CLFA) model are summarized in Table IV. All settings follow established design principles for efficient Transformer-based adaptation while remaining lightweight and easily integrable with the pretrained CLIP visual backbone. We place FusionAdapters at selected transformer layers (e.g., 6, 12, 18, and 24) of the ViT-B/32 encoder. Each adapter projects token embeddings into a 768-dimensional bottleneck, applies a tokenwise depthwise 1D convolution for local context modeling, fuses cross-layer descriptors, and re-injects the adapted features into the main stream via a small residual coefficient ($\alpha=0.1$). These choices balance computational efficiency, cross-layer information propagation, and handwriting-specific representation learning.

D. Cross-Task Zero-Shot Comparison and Discussion

To systematically analyze how handwriting task type affects zero-shot transferability, we compared our proposed CLFA with the multi-level baseline MVFA across the complete 25×25 zero-shot AUC matrices. Each matrix entry represents

TABLE IV
CLFA ARCHITECTURAL SETTINGS.

Parameter	Value
Visual Backbone	ViT-L-14-336
Adapter Layers (\mathcal{L})	[6, 12, 18, 24]
Hidden Dimension (C)	1024
Bottleneck Dimension (T)	768
Kernel Size (k)	3
Fusion Type	Cross-layer additive
Residual Coefficient (α)	0.1
Activation	LeakyReLU

the AUC achieved when training on task i and evaluating on an unseen task j , allowing analysis of both source-task generalization (row means) and target-task detectability (column means). This evaluation spans three functional task domains—graphic (G), copying (C), and memory/dictation (M)—which together reflect distinct visuomotor and cognitive demands relevant to Alzheimer’s disease (AD) handwriting assessment.

Overall performance: Across all off-diagonal train-test

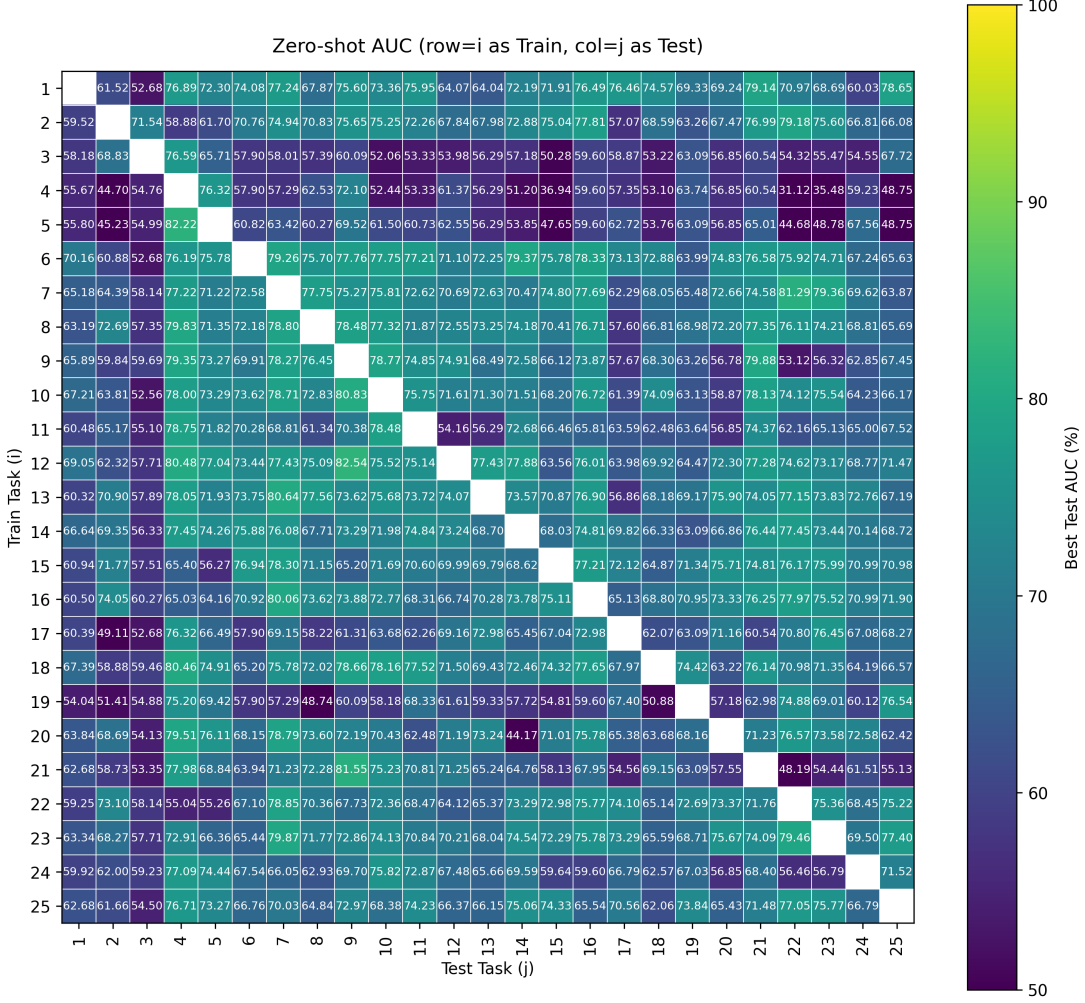


Fig. 5. Cross-task AUC matrix for zero-shot AD detection using MVFA. Rows denote training tasks; columns denote testing tasks. Higher off-diagonal values indicate stronger cross-task generalization.

TABLE V
PER-TASK CROSS-TASK MEAN AUC COMPARISON HIGHLIGHTING TRAINING-TASK GENERALIZATION (ROW MEANS) AND TESTING-TASK DETECTABILITY (COLUMN MEANS). THE FIRST TWO ROWS LIST ROW MEANS FOR CLFA AND MVFA. THE LAST TWO ROWS LIST COLUMN MEANS FOR CLFA AND MVFA.

	1	2	3	4	5	6	7	8	9	10	11	12	13	14	15	16	17	18	19	20	21	22	23	24	25
Row mean (CLFA)	71.39	71.18	65.09	56.49	59.58	73.89	72.87	72.15	71.16	71.94	71.36	74.39	72.62	72.34	70.33	70.90	65.83	72.33	64.75	71.74	68.52	69.58	72.46	67.86	70.46
Row mean (MVFA)	70.97	69.75	58.75	54.94	58.57	72.71	71.40	71.58	68.25	70.48	65.70	71.86	70.87	70.18	70.85	65.19	71.19	61.15	69.04	64.48	68.89	71.17	65.67	69.02	
Column mean (CLFA)	62.68	65.72	58.70	76.35	70.59	68.63	73.36	69.75	72.63	72.10	70.68	68.80	67.94	69.74	69.59	74.53	67.35	65.92	68.44	69.23	72.73	73.63	73.68	68.27	70.18
Column mean (MVFA)	62.18	62.80	56.80	75.06	70.06	67.95	73.10	68.45	72.55	71.11	69.93	67.57	66.95	68.29	66.07	71.58	64.84	64.80	66.71	65.99	72.44	68.36	68.08	66.24	67.07

pairs, CLFA achieves an average zero-shot AUC of **69.1%**, outperforming MVFA (**67.7%**) by **+1.85%**. Performance gains are distributed across nearly all tasks, reflecting CLFA’s ability to unify stroke-level motor dynamics, spatial layout, and linguistic content under a shared vision–language embedding space.

Source-task (row-mean) comparison: As training sources, CLFA improves cross-task transferability for all handwriting tasks. The most pronounced improvements appear in tasks emphasizing continuous visuomotor planning and trajectory regularity, where AD-related fine-motor instability typically impairs learning of transferable representations.

The top three gains occur in:

- **Task 3 (Join two points with a vertical line):** CLFA achieves a mean AUC of **59.13%** vs. 52.80% (+6.34%). Although seemingly simple, vertical line drawing tests fine-motor steadiness and proprioceptive consistency. Early AD patients frequently exhibit increased micro-tremor and reduced vertical stability due to impaired visuomotor feedback. CLFA’s depthwise 1D convolution enhances local stroke smoothness modeling, allowing the model to capture these subtle trajectory deviations and generalize them to other stroke-dominant tasks.
- **Task 11 (Copy the word “foglio” above a line):** CLFA attains **71.36%** vs. 65.70% (+5.66%). This task emphasizes vertical alignment and inter-letter spacing

along a fixed baseline—skills often degraded in AD owing to visuospatial disorganization and sensorimotor noise. CLFA’s cross-layer fusion effectively integrates low-level stroke cues with higher-level spatial layout features, producing representations that remain stable across handwriting styles and tasks.

- **Task 21 (Retrace a complex form):** CLFA reaches **65.45%** vs. 61.04% (+4.04%). Complex-form tracing requires coordinated visuospatial planning and continuous trajectory reproduction over long temporal spans. AD-related executive deficits lead to fragmented strokes and closure errors in such patterns. By hierarchically combining local token dynamics with global shape context, CLFA better encodes these deviations, yielding superior cross-task transfer compared with MVFA.

Overall, these improvements concentrate in tasks that probe either *micro-level stability* (Tasks 3 and 11) or *macro-level planning* (Task 21)—two domains that deteriorate early in AD. The consistent positive gains and absence of negative transfer confirm that CLFA’s hierarchical feature integration promotes stable, generalized learning of handwriting irregularities without overfitting to a specific task or trajectory pattern.

Target-task (column-mean) comparison: When used as unseen test targets, CLFA consistently achieves higher detectability across nearly all tasks, reflecting stronger zero-shot alignment between textual prompts and visual stroke evidence. With the largest margins observed in tasks requiring spatial closure, sequencing regularity, or multi-stroke integration.

The three most improved targets are:

- **Task 23 (Write a telephone number under dictation):** CLFA achieves an average AUC of **69.43%** vs. 63.84% (+5.59%). This task combines auditory comprehension, working-memory maintenance, and motor sequencing under time pressure. Early AD patients often struggle to retain multi-digit sequences, producing spacing errors, omissions, or rhythm irregularities. By fusing token-level motion patterns across network layers, CLFA better captures the temporal regularity and spacing coherence associated with intact cognitive control.
- **Task 22 (Copy a telephone number):** CLFA attains **69.77%** vs. 64.51% (+5.26%). Although visually similar to Task 23, this variant removes the auditory component, isolating visuomotor precision and sequential motor planning. CLFA’s cross-layer fusion enhances sensitivity to inter-symbol spacing and numerical alignment, effectively reflecting the deterioration of executive sequencing and fine-motor synchronization typical of AD handwriting.
- **Task 15 (Copy in reverse the word “bottiglia”):** CLFA reaches **66.07%** vs. 62.56% (+3.52%). Reverse copying taxes working-memory updating and directional planning—patients must maintain letter order while executing movements in a mirrored sequence. CLFA’s depthwise 1D convolution captures the small directional hesitations and inter-letter timing irregularities that arise from impaired cognitive–motor coupling in AD, yielding clearer separation between normal and pathological writing.

Overall, these results confirm that CLFA’s improvements concentrate on *sequence-driven* and *rule-based* writing behaviors—exactly those most affected by AD’s decline in executive and working-memory functions. The gains on both telephone-number and reversed-word tasks illustrate that the model not only detects visual–spatial irregularities but also encodes higher-order sequencing errors. No target task exhibits decreased AUC, confirming the robustness of CLFA’s zero-shot generalization. Figure 6 visualizes the per-task performance differences between CLFA and MVFA.

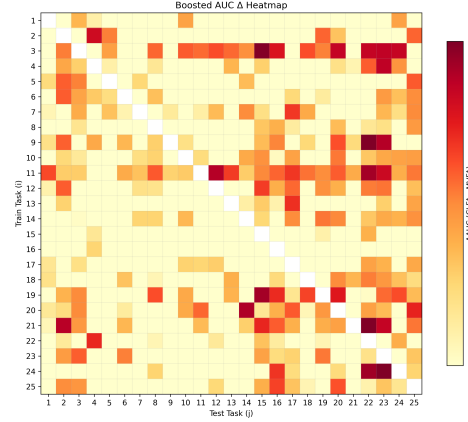


Fig. 6. The performance comparison heatmap between CLFA and MVFA

Mechanistic insight: CLFA’s advantage arises from three structural innovations that directly align with the dynamics of human handwriting:

- **Depthwise token convolution** introduces local temporal sensitivity along the stroke sequence, enabling the model to capture subtle tremor-like fluctuations and incomplete closures—fine-motor irregularities that MVFA’s pure transformer attention tends to smooth out.
- **Cross-layer feature fusion** transmits low-level pen-movement features upward to higher representational levels, improving semantic–motor alignment across tasks of different complexity (e.g., line vs. word copying). This mechanism particularly benefits tasks such as 11, 15, and 22, where linguistic and motor features co-occur.
- **Residual retargeting with adaptive scaling** balances CLIP’s pretrained visual–semantic priors with handwriting-specific adaptations, maintaining stable transferability across heterogeneous writing domains.

Neurocognitive interpretation: Statistical analysis of the top-100 cross-task improvements reveals that CLFA’s largest gains are not random but follow clear neurofunctional patterns consistent with known AD pathophysiology. More than two-thirds of the strongest occur between tasks bridging graphic (G) and copying (C) categories, while about one-fifth link graphic or copying to memory/dictation (M) tasks. This indicates that CLFA particularly enhances the transfer of visuomotor representations toward cognitively demanding linguistic or semantic tasks—an ability essential for modeling handwriting impairments in early AD.

(1) *Visuospatial–executive dysfunction:* Cross-domain transfers such as complex-form tracing → telephone-number copy-

ing (21→22, +23.1%) and clock drawing → number dictation (24→23, +20.91%) dominate the highest gains. These tasks jointly require global spatial planning, symmetry maintenance, and sequential execution—functions strongly dependent on parietal–frontal coordination, which deteriorates early in AD. CLFA’s cross-layer fusion preserves curvature continuity and spatial layout cues, allowing the model to better detect subtle planning disorganization and spatial closure errors across tasks.

(2) *Motor–language coupling*: Pairs such as cursive “le” → telephone-number copying (9→22, +20.52%) and line drawing → reversed-word copying (3→15, +19.59%) illustrate that CLFA excels when the source task encodes rhythmic motor continuity and the target demands sequential symbol generation. Across the top-100 pairs, over 40% involve at least one copying-related task, showing that CLFA more effectively maps low-level motor dynamics (stroke timing, inter-symbol spacing) onto high-level linguistic structure. This corresponds to improved modeling of handwriting rhythm, hesitation, and inter-letter transitions—key indicators of language–motor disintegration in AD.

(3) *Fine-motor and feedback stability*: Several top-ranked gains (e.g., 11→12, +15.87%; 3→24, +14.31%; 11→1, +8.18%) involve baseline-constrained or repetitive-motion tasks, where smooth stroke control and pressure consistency are critical. CLFA’s depthwise token convolution captures micro-kinematic dependencies and tremor-like irregularities that MVFA’s transformer attention tends to overlook. This leads to higher sensitivity to vertical drift, pen-lift frequency, and curvature noise—fine-motor deficits that frequently precede cognitive symptoms in AD.

In summary, statistical patterns from the top-100 improvement pairs show that CLFA enhances three interconnected functional domains—*visuospatial planning*, *motor–language coordination*, and *fine-motor regulation*. By reinforcing transfer between geometric tracing, copying, and dictation tasks, CLFA aligns more closely with the hierarchical progression of handwriting impairments in AD, reflecting a model that not only performs better numerically but also mirrors underlying neurocognitive decline. The count distribution of each task leading to C/G/M target categories within the Top-100 shown in Figure 7.

E. Task-Specific Cross-Task Relations and Discussion

We analyze the full cross-task matrix (rows = training sources, columns = unseen targets) and relate the strongest relations to task demands and Alzheimer’s disease (AD) handwriting markers.

Global patterns: High-scoring pairs concentrate around (i) copying (C) sources that instill transferable priors on stroke continuity, inter-symbol spacing, and line alignment, and (ii) graphic or numeric/dictation targets that magnify differences in spatial closure (circles, complex forms) and sequential regularity (phone numbers). Representative top relations include 9→4 (cursive bigram → circle-6cm), 12→9 (copy “mamma” → cursive bigram), 7→22/23 (letters on rows → phone copying/dictation), 21→4/9 (complex form → circle/cursive),

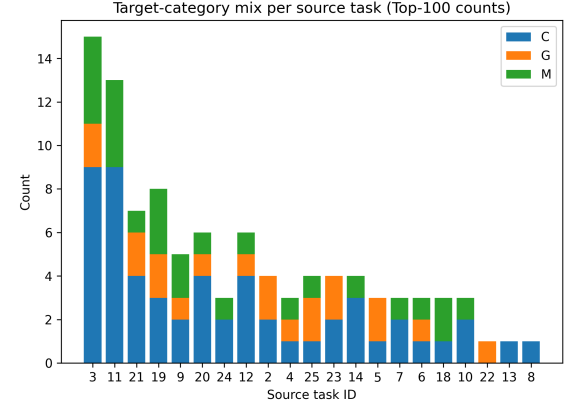


Fig. 7. The count distribution of each task leading to C/G/M target categories within the Top-100

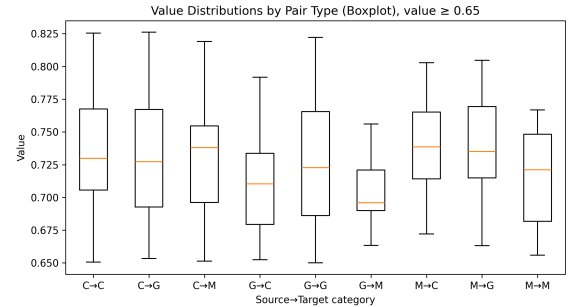


Fig. 8. Box-and-whisker plots for category distribution

and 24→23/22 (clock → number dictation/copying). These routes jointly indicate that CLFA converts motor–rhythmic constraints learned from C sources into robust signals for G/C/M targets that stress closure, layout, and sequencing.

Sources that generalize best: (Cursive, word-level, and baseline-constrained copying) are the most effective trainers:

- **Task 9 (Cursive bigram “le”, C):** yields many top routes (e.g., 9→4, 9→21, 9→10/16/22/23). Fluent stroke connectivity and timing learned here transfer to curvature uniformity (G) and digit spacing (C/M).
- **Task 12 (Copy “mamma”, C):** strongly exports to cursive/graphic/numeric targets (12→9/4/22/23/16). CLFA’s cross-layer fusion carries low-level micro-kinematics into higher-level word-shape and sequencing.
- **Task 6/7/11 (Copy l/m/p; letters on rows; “foglio” on a line, C):** repeatedly appear as sources toward C/G/M targets (e.g., 7→22/23/16/21; 11→10/22/23). These tasks strengthen priors on baseline adherence, inter-line alignment, and micro-variations among similar graphemes.
- **Task 21/24 (Complex form; Clock, G):** act as geometric scaffolds (21/24→22/23/4/10/16), exporting spatial closure, symmetry, and global layout to symbol sequencing and dictation.
- **Task 20/18 (Sentence dictation; Object naming, M):** provide semantic–motor bridges (20/18→22/16/9/4/21), improving cross-modal alignment under cognitive load.

AD link: these sources capture precisely the domains com-

promised early in AD—stroke rhythm and spacing (motor–language coupling), visuospatial planning and closure (executive dysfunction), and cross-modal control (auditory–semantic to motor).

Targets that are easiest to detect: Several tasks consistently receive strong transfer and thus serve as discriminative targets:

- **Task 4 (Circle 6 cm, G):** repeatedly reached from C/M/G sources (9/12/8/21/24/20→4). Circular closure amplifies deficits in curvature continuity, drift, and tremor-like noise.
- **Task 22/23 (Copy/dictate phone number, C/M):** attract high-performing routes from 7/9/12/14/20/21/1 (e.g., 7/9/12/14/20→22; 24/21/10/12→23). These tasks are sensitive to sequencing regularity, spacing, and working-memory constraints.
- **Task 9/21/16 (Cursive bigram; Complex form; Reverse “casa”):** expose deficits in stroke continuity (9), global organization (21), and executive control for reversed ordering (16).

AD link: these targets reveal canonical dysgraphia signatures—loss of smoothness and closure (4/21), irregular spacing and hesitation (22/23/9), and sequencing disorganization (16).

Category-level transfer: From the full matrix, three robust patterns emerge, Box-and-whisker plots for category distribution (only values greater than 65% are counted) are shown in Figure 8.:

- 1) **C→G and C→C dominate:** copying sources (9/12/6/7/11) generalize broadly to graphic and copying targets (4/21/9/7/22/23), reflecting the portability of rhythm, spacing, and baseline priors.
- 2) **G→C/M is strong:** complex/clock sources (21/24) export global layout and closure to numeric/dictation targets (22/23) and to lexical copying (10/16/11).
- 3) **M→C/G is substantial:** dictation/naming sources (20/18) improve detection on symbol sequencing and geometric closure targets (22/16/9/4/21), evidencing enhanced semantic–motor coupling.

Practical guidance: For training with minimal yet informative sources, prioritize **C**: {9, 12, 6, 7, 11}, and complement with **G**: {21, 24} and **M**: {20}. The Top-3 Route Point Map for Each Task shown in figure 9, the Hit Rate–Performance Dual-Axis Chart shown in figure 10. For zero-shot evaluation, a compact but sensitive target set is {4, 22, 23, 9, 21, 16}, jointly spanning visuospatial closure, stroke rhythm/spacing, and sequencing under cognitive load.

Clinical interpretation: The strongest relations map closely onto AD pathophysiology: (i) visuospatial–executive dysfunction (enhanced closure/planning cues transferring across G↔C/M), (ii) impaired motor–language coupling (improved capture of rhythm, inter-letter transitions, and spacing regularity), and (iii) fine-motor instability (sensitivity to micro-kinematic fluctuations and baseline drift). In sum, CLFA does not merely raise AUCs; it strengthens functional bridges across motor, visuospatial, and linguistic processes, yielding task-to-task transfer that is both quantitatively superior and neurocognitively meaningful.

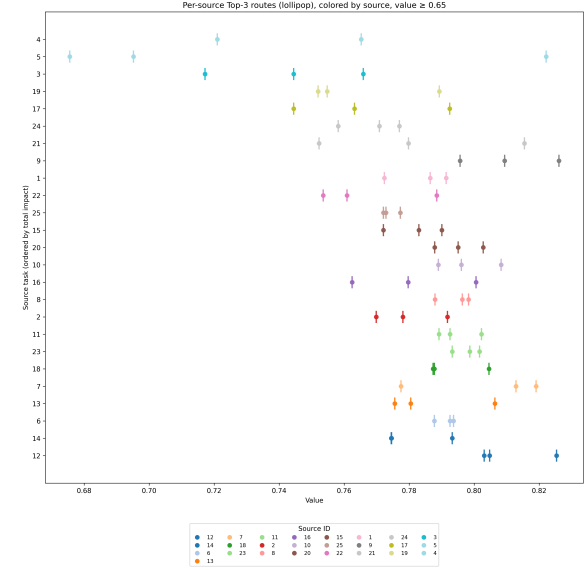


Fig. 9. Top-3 Route Point Map for Each Task

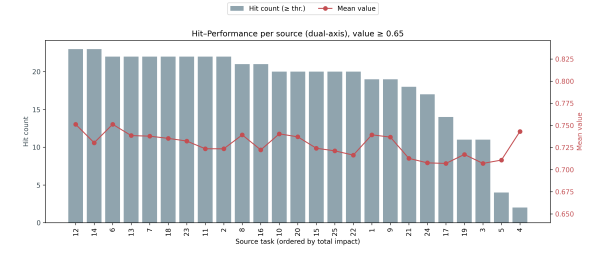


Fig. 10. Hit Rate–Performance Dual-Axis Chart (Bar = Number of Hits, Line = Average Value)

VI. CONCLUSION

In this study, we presented a systematic exploration of handwriting-based Alzheimer’s disease (AD) detection from a cross-task perspective. Departing from previous works that focus on single-task performance, we examined how different handwriting tasks influence zero-shot generalization and diagnostic sensitivity. To enable this analysis, we introduced the Cross-Layer Fusion Adapter (CLFA), a lightweight vision–language adaptation framework that repurposes CLIP for handwriting-based medical screening. CLFA embeds tokenwise depthwise 1D convolution and cross-layer fusion within the visual encoder, aligning low-level stroke dynamics with higher-level layout and shape representations, while preserving pretrained semantic knowledge through lightweight residual retargeting.

The proposed architecture efficiently captures the fine-grained motor irregularities characteristic of early AD—such as stroke discontinuity, curvature fluctuation, and spatial drift—without relying on task-specific prompts or external supervision. Its cross-layer fusion mechanism propagates handwriting cues across multiple representational depths, allowing the model to generalize from one writing task to unseen ones in a zero-shot manner. Compared with the MVFA baseline, CLFA consistently improves cross-task AUCs, particularly in

tasks requiring continuous visuospatial control or sequential language–motor coordination (e.g., circle tracing, complex figure copying, phone-number copying, and reversed writing).

Our comprehensive 25×25 zero-shot analysis revealed that cross-task transferability is not random but structured by task mechanics. Copy-based tasks, which combine linguistic planning and fine-motor execution, serve as the most reliable training sources, whereas closure- and sequencing-intensive tasks (e.g., large-circle tracing, complex figure copying, and reversed copying) emerge as the most diagnostically sensitive targets. These results quantitatively demonstrate that handwriting tasks engaging both cognitive–linguistic and visuospatial–executive functions yield stronger discriminative signals for AD, offering evidence-based guidance for future handwriting screening protocols.

Despite its promising generalization ability, this study has several limitations. First, although the dataset covers diverse task types, it remains limited in demographic representation and writing conditions, which may constrain population-level generalizability. Second, CLFA currently focuses on image-level representations; incorporating the temporal dynamics of pen trajectories could further enhance interpretability and sensitivity to micro-motor fluctuations. Third, the accuracy of vision–language models (VLMs) often relies on time-consuming and expertise-dependent prompt engineering. Future work will extend toward few-shot personalization, multimodal fusion (e.g., integrating handwriting with speech or eye-tracking), and more efficient prompt-context learning to enable more comprehensive cognitive assessment in real-world settings.

In summary, this work provides both a methodological contribution—a novel, efficient vision–language adapter for handwriting analysis—and a scientific insight: handwriting task design fundamentally shapes cross-task generalization in AD detection. By bridging large-scale vision–language pretraining with neurocognitive task analysis, our framework opens new avenues for explainable and scalable digital biomarkers of neurodegenerative diseases.

REFERENCES

- [1] M. A. El-Yacoubi, S. Garcia-Salicetti, C. Kahindo, A.-S. Rigaud, V. Cristancho-Lacroix, From aging to early-stage alzheimer’s: uncovering handwriting multimodal behaviors by semi-supervised learning and sequential representation learning, *Pattern Recognition* 86 (2019) 112–133.
- [2] A. K. Singhal, V. Naithani, O. P. Bangar, Medicinal plants with a potential to treat alzheimer and associated symptoms, *International Journal of Nutrition, Pharmacology, Neurological Diseases* 2 (2) (2012) 84–91.
- [3] A. Association, 2019 alzheimer’s disease facts and figures, *Alzheimer’s & dementia* 15 (3) (2019) 321–387.
- [4] A. S. Buchman, D. A. Bennett, Loss of motor function in preclinical alzheimer’s disease, *Expert review of neurotherapeutics* 11 (5) (2011) 665–676.
- [5] M. J. Armstrong, I. Litvan, A. E. Lang, T. H. Bak, K. P. Bhatia, B. Borroni, A. L. Boxer, D. W. Dickson, M. Grossman, M. Hallett, et al., Criteria for the diagnosis of corticobasal degeneration, *Neurology* 80 (5) (2013) 496–503.
- [6] Y. Zhang, Y. Chen, H. Yu, Z. Lv, X. Yang, C. Hu, T. Zhang, What can “drag & drop” tell? detecting mild cognitive impairment by hand motor function assessment under dual-task paradigm, *International Journal of Human-Computer Studies* 145 (2021) 102547.
- [7] R. C. Petersen, O. Lopez, M. J. Armstrong, T. S. Getchius, M. Ganguli, D. Gloss, G. S. Gronseth, D. Marson, T. Pringsheim, G. S. Day, et al., Practice guideline update summary: Mild cognitive impairment: Report of the guideline development, dissemination, and implementation subcommittee of the american academy of neurology, *Neurology* 90 (3) (2018) 126–135.
- [8] M. Ewers, K. Buerger, S. Teipel, P. Scheltens, J. Schroder, R. Zinkowski, F. Bouwman, P. Schonknecht, N. Schoonenboom, N. Andreasen, et al., Multicenter assessment of csf-phosphorylated tau for the prediction of conversion of mci, *Neurology* 69 (24) (2007) 2205–2212.
- [9] M. S. Baek, H.-K. Kim, K. Han, H.-S. Kwon, H. K. Na, C. H. Lyoo, H. Cho, Annual trends in the incidence and prevalence of alzheimer’s disease in south korea: a nationwide cohort study, *Frontiers in Neurology* 13 (2022) 883549.
- [10] E. Nichols, J. D. Steinmetz, S. E. Vollset, K. Fukutaki, J. Chalek, F. Abd-Allah, A. Abdoli, A. Abualhasan, E. Abu-Gharbieh, T. T. Akram, et al., Estimation of the global prevalence of dementia in 2019 and forecasted prevalence in 2050: an analysis for the global burden of disease study 2019, *The Lancet Public Health* 7 (2) (2022) e105–e125.
- [11] J. M. Long, D. M. Holtzman, Alzheimer disease: an update on pathobiology and treatment strategies, *Cell* 179 (2) (2019) 312–339.
- [12] S. C. Burnham, P. Coloma, Q.-X. Li, S. Collins, G. Savage, S. Laws, J. Doecke, P. Maruff, R. Martins, D. Ames, et al., Application of the nia-aa research framework: towards a biological definition of alzheimer’s disease using cerebrospinal fluid biomarkers in the aibl study, *The Journal of Prevention of Alzheimer’s Disease* 6 (2019) 248–255.
- [13] G. Gosztolya, V. Vincze, L. Tóth, M. Pákáski, J. Kálmán, I. Hoffmann, Identifying mild cognitive impairment and mild alzheimer’s disease based on spontaneous speech using asr and linguistic features, *Computer Speech & Language* 53 (2019) 181–197.
- [14] X.-t. Ma, L.-l. Yao, S.-w. Liu, X.-f. Weng, R.-y. Bao, Y.-f. Yang, Y.-f. Li, Y.-y. Sun, D. Xu, Z.-y. Jia, et al., The link between eye movements and cognitive function in mild to moderate alzheimer’s disease, *Experimental Brain Research* 243 (1) (2025) 39.
- [15] J.-U. Bang, S.-H. Han, B.-O. Kang, Alzheimer’s disease recognition from spontaneous speech using large language models, *ETRI Journal* 46 (1) (2024) 96–105.
- [16] S. Saha, K. Jindal, D. Shakti, S. Tewary, V. Sardana, Chirplet transform-based machine-learning approach to

wards classification of cognitive state change using galvanic skin response and photoplethysmography signals, *Expert Systems* 39 (6) (2022) e12958.

[17] Y. Yamada, K. Shinkawa, M. Kobayashi, V. Caggiano, M. Nemoto, K. Nemoto, T. Arai, Combining multimodal behavioral data of gait, speech, and drawing for classification of alzheimer's disease and mild cognitive impairment, *Journal of Alzheimer's Disease* 84 (1) (2021) 315–327.

[18] L. E. Hebert, J. L. Bienias, J. J. McCann, P. A. Scherr, R. S. Wilson, D. A. Evans, Upper and lower extremity motor performance and functional impairment in alzheimer's disease, *American Journal of Alzheimer's Disease & Other Dementias®* 25 (5) (2010) 425–431.

[19] A. S. Buchman, P. A. Boyle, R. S. Wilson, Y. Tang, D. A. Bennett, Frailty is associated with incident alzheimer's disease and cognitive decline in the elderly, *Psychosomatic medicine* 69 (5) (2007) 483–489.

[20] P. A. Boyle, A. S. Buchman, R. S. Wilson, S. E. Leurgans, D. A. Bennett, Physical frailty is associated with incident mild cognitive impairment in community-based older persons, *Journal of the American Geriatrics Society* 58 (2) (2010) 248–255.

[21] J. H. Yan, S. Rountree, P. Massman, R. S. Doody, H. Li, Alzheimer's disease and mild cognitive impairment deteriorate fine movement control, *Journal of Psychiatric Research* 42 (14) (2008) 1203–1212.

[22] D. Impedovo, G. Pirlo, G. Vessio, Dynamic handwriting analysis for supporting earlier parkinson's disease diagnosis, *Information* 9 (10) (2018) 247.

[23] N.-Y. Yu, S.-H. Chang, Kinematic analyses of graphomotor functions in individuals with alzheimer's disease and amnestic mild cognitive impairment, *Journal of Medical and Biological Engineering* 36 (2016) 334–343.

[24] N. D. Cilia, C. De Stefano, F. Fontanella, A. S. Di Freca, An experimental protocol to support cognitive impairment diagnosis by using handwriting analysis, *Procedia Computer Science* 141 (2018) 466–471.

[25] J. Garre-Olmo, M. Faúndez-Zanuy, K. López-de Ipiña, L. Calvó-Perxas, O. Turró-Garriga, Kinematic and pressure features of handwriting and drawing: preliminary results between patients with mild cognitive impairment, alzheimer disease and healthy controls, *Current Alzheimer Research* 14 (9) (2017) 960–968.

[26] J. Kawa, A. Bednorz, P. Stepień, J. Derejczyk, M. Bugdol, Spatial and dynamical handwriting analysis in mild cognitive impairment, *Computers in Biology and Medicine* 82 (2017) 21–28.

[27] A. Schröter, R. Mergl, K. Bürger, H. Hampel, H.-J. Möller, U. Hegerl, Kinematic analysis of handwriting movements in patients with alzheimer's disease, mild cognitive impairment, depression and healthy subjects, *Dementia and geriatric cognitive disorders* 15 (3) (2003) 132–142.

[28] M. A. Myszczynska, P. N. Ojamies, A. M. Lacoste, D. Neil, A. Saffari, R. Mead, G. M. Hautbergue, J. D. Holbrook, L. Ferraiuolo, Applications of machine learning to diagnosis and treatment of neurodegenerative diseases, *Nature reviews neurology* 16 (8) (2020) 440–456.

[29] C. Kahindo, M. A. El-Yacoubi, S. Garcia-Salicetti, A.-S. Rigaud, V. Cristancho-Lacroix, Characterizing early-stage alzheimer through spatiotemporal dynamics of handwriting, *IEEE Signal Processing Letters* 25 (8) (2018) 1136–1140.

[30] H. Qi, R. Zhang, Z. Wei, C. Zhang, L. Wang, Q. Lang, K. Zhang, X. Tian, A study of auxiliary screening for alzheimer's disease based on handwriting characteristics, *Frontiers in aging neuroscience* 15 (2023) 1117250.

[31] J. Chai, R. Wu, A. Li, C. Xue, Y. Qiang, J. Zhao, Q. Zhao, Q. Yang, Classification of mild cognitive impairment based on handwriting dynamics and qeeg, *Computers in biology and medicine* 152 (2023) 106418.

[32] Q. Dao, M. A. El-Yacoubi, A.-S. Rigaud, Detection of alzheimer disease on online handwriting using 1d convolutional neural network, *IEEE Access* 11 (2022) 2148–2155.

[33] N. Mwamsojo, F. Lehmann, M. A. El-Yacoubi, K. Merghem, Y. Frignac, B.-E. Benkelfat, A.-S. Rigaud, Reservoir computing for early stage alzheimer's disease detection, *IEEE Access* 10 (2022) 59821–59831.

[34] P. Erdogmus, A. T. Kabakus, The promise of convolutional neural networks for the early diagnosis of the alzheimer's disease, *Engineering Applications of Artificial Intelligence* 123 (2023) 106254.

[35] C. Gong, H. Qin, M. A. El-Yacoubi, Hybrid transformer for early alzheimer's detection: Integration of handwriting-based 2d images and 1d signal features, *IEEE Journal of Biomedical and Health Informatics*.

[36] X. Ma, G. Fang, X. Wang, Deepcache: Accelerating diffusion models for free, in: *Proceedings of the IEEE/CVF conference on computer vision and pattern recognition*, 2024, pp. 15762–15772.

[37] T. Yu, Z. Lu, X. Jin, Z. Chen, X. Wang, Task residual for tuning vision-language models, in: *Proceedings of the IEEE/CVF conference on computer vision and pattern recognition*, 2023, pp. 10899–10909.

[38] X. Yang, X. Wang, Diffusion model as representation learner, in: *Proceedings of the IEEE/CVF International Conference on Computer Vision*, 2023, pp. 18938–18949.

[39] J. Zhu, G. Pang, Toward generalist anomaly detection via in-context residual learning with few-shot sample prompts, in: *Proceedings of the IEEE/CVF conference on computer vision and pattern recognition*, 2024, pp. 17826–17836.

[40] A. Radford, J. W. Kim, C. Hallacy, A. Ramesh, G. Goh, S. Agarwal, G. Sastry, A. Askell, P. Mishkin, J. Clark, et al., Learning transferable visual models from natural language supervision, in: *International conference on machine learning*, PMLR, 2021, pp. 8748–8763.

[41] G. Goh, N. Cammarata, C. Voss, S. Carter, M. Petrov, L. Schubert, A. Radford, C. Olah, Multimodal neurons in artificial neural networks, *Distill* 6 (3) (2021) e30.

[42] R. Taori, A. Dave, V. Shankar, N. Carlini, B. Recht, L. Schmidt, Measuring robustness to natural distribution

shifts in image classification, *Advances in Neural Information Processing Systems* 33 (2020) 18583–18599.

[43] C. Huang, A. Jiang, J. Feng, Y. Zhang, X. Wang, Y. Wang, Adapting visual-language models for generalizable anomaly detection in medical images, in: *Proceedings of the IEEE/CVF Conference on Computer Vision and Pattern Recognition*, 2024, pp. 11375–11385.

[44] J. Meng, X. Huo, H. Zhao, L. Zhang, X. Wang, Y. Wang, Image-based handwriting analysis for disease diagnosis, in: *2022 41st Chinese Control Conference (CCC)*, IEEE, 2022, pp. 4058–4062.

[45] N. D. Cilia, G. De Gregorio, C. De Stefano, F. Fontanella, A. Marcelli, A. Parziale, Diagnosing alzheimer’s disease from on-line handwriting: A novel dataset and performance benchmarking, *Engineering Applications of Artificial Intelligence* 111 (2022) 104822.

[46] C. R. Pereira, D. R. Pereira, G. H. Rosa, V. H. Albuquerque, S. A. Weber, C. Hook, J. P. Papa, Handwritten dynamics assessment through convolutional neural networks: An application to parkinson’s disease identification, *Artificial intelligence in medicine* 87 (2018) 67–77.

[47] C. Taleb, L. Likforman-Sulem, C. Mokbel, M. Khachab, Detection of parkinson’s disease from handwriting using deep learning: a comparative study, *Evolutionary Intelligence* (2023) 1–12.

[48] M. Diaz, M. Moetesum, I. Siddiqi, G. Vessio, Sequence-based dynamic handwriting analysis for parkinson’s disease detection with one-dimensional convolutions and bigrus, *Expert Systems with Applications* 168 (2021) 114405.

[49] N. D. Cilia, T. D’Alessandro, C. De Stefano, F. Fontanella, M. Molinara, From online handwriting to synthetic images for alzheimer’s disease detection using a deep transfer learning approach, *IEEE Journal of Biomedical and Health Informatics* 25 (12) (2021) 4243–4254.

[50] N. D. Cilia, T. D’Alessandro, C. De Stefano, F. Fontanella, Deep transfer learning algorithms applied to synthetic drawing images as a tool for supporting alzheimer’s disease prediction, *Machine Vision and Applications* 33 (3) (2022) 49.

[51] J. Jeong, Y. Zou, T. Kim, D. Zhang, A. Ravichandran, O. Dabeer, Winclip: Zero-/few-shot anomaly classification and segmentation, in: *Proceedings of the IEEE/CVF Conference on Computer Vision and Pattern Recognition*, 2023, pp. 19606–19616.

[52] A. Costanzino, P. Z. Ramirez, G. Lisanti, L. Di Stefano, Multimodal industrial anomaly detection by crossmodal feature mapping, in: *Proceedings of the IEEE/CVF Conference on Computer Vision and Pattern Recognition*, 2024, pp. 17234–17243.

[53] J. Zhu, C. Ding, Y. Tian, G. Pang, Anomaly heterogeneity learning for open-set supervised anomaly detection, in: *Proceedings of the IEEE/CVF conference on computer vision and pattern recognition*, 2024, pp. 17616–17626.

[54] J. Bao, H. Sun, H. Deng, Y. He, Z. Zhang, X. Li, Bmad: Benchmarks for medical anomaly detection, in: *Proceedings of the IEEE/CVF Conference on Computer Vision and Pattern Recognition*, 2024, pp. 4042–4053.

[55] A. Jiang, C. Huang, Q. Cao, S. Wu, Z. Zeng, K. Chen, Y. Zhang, Y. Wang, Multi-scale cross-restoration framework for electrocardiogram anomaly detection, in: *International Conference on Medical Image Computing and Computer-Assisted Intervention*, Springer, 2023, pp. 87–97.

[56] J. Zhang, Y. Xie, G. Pang, Z. Liao, J. Verjans, W. Li, Z. Sun, J. He, Y. Li, C. Shen, et al., Viral pneumonia screening on chest x-rays using confidence-aware anomaly detection, *IEEE transactions on medical imaging* 40 (3) (2020) 879–890.

[57] K. Zhou, Y. Xiao, J. Yang, J. Cheng, W. Liu, W. Luo, Z. Gu, J. Liu, S. Gao, Encoding structure-texture relation with p-net for anomaly detection in retinal images, in: *European conference on computer vision*, Springer, 2020, pp. 360–377.

[58] K. Zhou, J. Li, W. Luo, Z. Li, J. Yang, H. Fu, J. Cheng, J. Liu, S. Gao, Proxy-bridged image reconstruction network for anomaly detection in medical images, *IEEE Transactions on Medical Imaging* 41 (3) (2021) 582–594.

[59] Y. Rao, W. Zhao, G. Chen, Y. Tang, Z. Zhu, G. Huang, J. Zhou, J. Lu, Denseclip: Language-guided dense prediction with context-aware prompting, in: *Proceedings of the IEEE/CVF conference on computer vision and pattern recognition*, 2022, pp. 18082–18091.

[60] Y. Zhong, J. Yang, P. Zhang, C. Li, N. Codella, L. H. Li, L. Zhou, X. Dai, L. Yuan, Y. Li, et al., Regionclip: Region-based language-image pretraining, in: *Proceedings of the IEEE/CVF conference on computer vision and pattern recognition*, 2022, pp. 16793–16803.